Special Section: Digital Soil Mapping

Angela Lausch*
Steffen Zacharias
Claudia Dierke
Marion Pause
Ingolf Kühn
Daniel Doktor
Peter Dietrich
Ulrike Werban

Spatial vegetation patterns can be used as a proxies of the underlying soil and soil water conditions. The study examines the use of hyperspectral remote sensing techniques for quantifying geophysical parameters from the hyperspectral reflectance of the vegetation canopy. The best prediction of EMI and gamma-ray measurements was found by a combination of elevation and hyperspectral remote sensing information.

A. Lausch and D. Doktor, Dep. of Computational Landscape Ecology, UFZ Helmholtz Centre for Environmental Research, Permoserstr. 15/D-04318 Leipzig, Germany; S. Zacharias, C. Dierke, P. Dietrich, and U. Werban, Dep. of Monitoring and Exploration Technologies, UFZ Helmholtz Centre for Environmental Research, Permoserstr. 15/D-04318 Leipzig, Germany; M. Pause, WESS—Water and Earth System Science Competence Cluster, Univ. of Tübingen, Keplerstrasse 17, D-72074 Tübingen, Germany; and I. Kühn, Dep. of Community Ecology, UFZ Helmholtz Centre for Environmental Research, Theodor-Lieser-Str. 4, D-06120 Halle, Germany. *Corresponding author (angela.lausch@ufz.de).

Vadose Zone J.
doi:10.2136/vzj2012.0217
Received 31 Dec. 2012.

Analysis of Vegetation and Soil Patterns using Hyperspectral Remote Sensing, EMI, and Gamma-Ray Measurements

The identification of spatial and temporal patterns of soil properties and moisture structures is an important challenge in environmental and soil monitoring as well as for soil landscape model approaches. This work examines the use of hyperspectral remote sensing techniques for quantifying geophysical parameters from the hyperspectral reflectance of the vegetation canopy. These can be used as proxies of the underlying soil and soil water conditions. Different spectral index derivatives, single band reflectance, and spectral indices from the airborne hyperspectral sensor AISA were quantified and tested in univariate and multivariate regression models for their correlation with geophysical measurements with electromagnetic induction (EMI) and gamma-ray spectrometry. The best univariate models for predicting electrical conductivity based on spectral information were based on the vertical dipole of an EM38DD with an R^2 = 0.54 with the spectral index Normalized Pigments Reflectance Index (NPCI) as well as for the horizontal dipole of an EM38DD with an R^2 = 0.65 with the spectral index NPCI. For predicting soil characteristics measured with gamma-ray spectrometry we received the best model results for γTh with an R^2 = 0.55 with the spectral index NPCI and γK with an R^2 = 0.44 with the spectral index Triangular Vegetation Index (TVI) and NPCI. The combination of variables including the geographical elevation was tested as the input for a multivariate regression analysis. For EMI and gamma-ray measurements, the "elevation" was found to be the most predictive variable and an integration of spectral indices into the elevation-based model led to only a slight improvement in the predictive power for EMI. An improvement could be made to explain the variance of gamma-ray measurement signals by combining elevation and spectral information.

Abbreviations: CAI, cellulose absorption index; NPCI, normalized pigments reflectance index; PLS, partial least-squares; PSRI, plant senescence reflectance index; QP, quadrature phase; SWIR, short wave infrared; TVI, triangular vegetation index.

Soil heterogeneity is a key challenge when modeling the flow, transport, and turnover processes in the soil-landscape context. Reliable forecasts require profound knowledge about the variability of soil parameters and the functional heterogeneity in terrestrial systems. Therefore, methods are required to measure and assess the distribution and pattern of soil properties.

Quantifying and qualifying the spatial and temporal patterns of soil properties and moisture characteristics is still one of the central challenges in environmental monitoring. An adequate description of soil variability is an essential piece of information to put into ecological modeling, agriculture, and soil management (Bouma et al., 1999; Grayson and Blöschl, 2001; Lin et al., 2005, 2006; Schulz et al., 2006). Soil maps are the key to providing information about soil distribution, soil structures, underlying processes on scales appropriate for the modeling or management of soils and for linking, monitoring data, and understanding landscape characteristics (Bouma, 2009; Heuvelink and Webster, 2001; Lin et al., 2005; McBratney et al., 2003; Scull et al., 2003; van Egmond et al., 2009).

Soil characteristics and soil moisture patterns are important site conditions affecting biochemical–physical properties of plants and vegetation as a result of adaptation or plant stress (Feilhauer and Schmidtlein, 2011; King et al., 2012; Schmidtlein and Sassin, 2004). The functional reactions of plants and vegetation are controlled and influenced by a combination of soil properties including characteristics such as texture, salinity, pH-level, chemical composition, soil moisture patterns, and temperature (Tromp-van Meerveld and McDonnell, 2009; Li et al., 2011; Schmidtlein et al., 2012). The presence of functional

relationships between soil properties and vegetation patterns can clearly be observed from simple aerial photography and satellite images (Fig. 1).

Geophysical measurement techniques, such as ground-penetrating radars, soil-moisture sensor networks, electromagnetic induction, and remote sensing technologies, present an opportunity for collecting information about the spatial and temporal variation of soil properties covering a wide range of scales (Vereecken et al., 2008). In spite of the technological progress that has been made over recent decades, several obstacles still have to be overcome to meet the need for low-cost, high-resolution soil maps (van Egmond et al., 2009).

A main problem arises from the fact that the exact relationship between the sensed characteristics and the environmental quantity of interest is often only poorly known or difficult to extract from the sensed signal. The analysis of empirical relationships between those indirect parameters and the parameter of interest can be seen as a preliminary step toward a better understanding of the underlying processes. Data fusion approaches and the combination and incorporation of different kinds of data may present a promising solution for improving data interpretation and the prediction of soil properties (Kowalsky et al., 2004; Vereecken et al., 2008).

Remote sensing techniques are frequently used to map and assess the spatial variability of bare ground soil properties or states such as the content of soil organic matter, soil salinity, or soil moisture. In this way Ben-Dor et al. (2002) used airborne image spectrometer data such as DAIS-7915 to study soil properties and their spatial distribution, while Jarmer et al. (2005) used simple optical remote sensing sensors such as Landsat-TM to assess soil inorganic carbon in the Judean Desert. To obtain and assess spatial and multi-temporal surface soil moisture data over large areas both microwave remote sensing techniques (Jackson et al., 1976; Chang and Islam, 2000; Wigneron et al., 2003; Pause et al., 2012) as well as various optical sensors such as hyperspectral data (Haubrock et al., 2008) can be used.

To assess the soil heterogeneity of sites with vegetation from remote sensing, the use of indirect indicators is required (Wehrhan et al., 2001; Schmidtlein, 2005; Lausch et al., 2012, 2013a). The most frequently used indicators in this respect are (i) the "Ellenberg indicator values" of plants and (ii) a characterization of the "vitality" of plants and vegetation.

The "Ellenberg indicator values" rank plant species according to their occurrence along soil property gradients such as the water supply, pH characteristics, soil fertility, salinity, etc. (Ellenberg et al., 1991; Hill et al., 2000; Schmidtlein, 2005). In this way Schmidtlein (2005) was able to use a partial least-squares (PLS) regression to substantiate the spatial distribution of the soil attributes: water supply, soil pH, and soil fertility—as indicated by the Ellenberg values based on image spectroscopy with an R^2 of 0.68.

The "vitality" of plants and vegetation represents a combination of different factors. When plant species and plant communities are not optimally adapted to the existing phenological environment and its hydrological and chemical features, then they might show various indications of stress. Typical stress factors are changes in soil properties (nutrient and salinity stress) and changes in moisture conditions (water stress). Such stress factors can induce a change in the biochemical–physiological characteristics of plants and vegetation, which can be detected by remote sensing observation.

Fig. 1. Agricultural landscapes situated in Saxony-Anhalt, Germany; crops show considerable structural changes due to the specific soil conditions of the underlying substrate; image taken by A. Lausch (2010).

The most important functional reactions to stress which can be documented using remote sensing techniques are (i) changes in the composition and proportion of photosynthetically active pigments such as chlorophyll *a*, *b*, and xanthophylle (Hák et al., 1990; Miller et al., 2002; Zhang et al., 2008; Lausch et al., 2013b), (ii) changes in photosynthetic activity through the fluorescence effects in plants (Naumann et al., 2008; Zarco-Tejada et al., 2009), (iii) changes to the water status of the plant as well as the percentage of water in leaf cells (Eitel et al., 2006; Suárez et al., 2008; Zarco-Tejada et al., 2012), (iv) changes in cellulose and lignin content in the vegetation (Bannari et al., 2006; Swatantran et al., 2011), and (v) changes in plant transpiration, resulting in changes in leaf arrangement and geometry, stomata distribution as well as special protective mechanisms such as leaf hairs and cuticula (Claudio et al., 2006; Hernández-Clemente et al., 2011).

More recently, researchers have started to investigate the potential of using remote sensing to analyze structural and functional relationships between soil heterogeneity and state variables (e.g., soil moisture) by using remotely sensed information about vegetation patterns and physiological reactions of plants (Li et al., 2011). Shrestha (2006) used the Landsat Enhanced Thematic Mapper Plus (ETM+) to predict soil electrical conductivity (6_a). He used linear regression modeling and achieved a relatively modest correlation between 6_a and the spectral band 7 of 0.48. Li et al. (2011) used a handheld field spectrometer ASD FieldSpec Pro to examine the relationship between ground-based assessments of the hyperspectral reflectance of wetland plants and the apparent electrical conductivity of the underlying soils in alkaline wetland habitats. They achieved the best model for predicting the 6_a with uni- and multivariate regression models with an R^2 of 0.59. Bajwa et al. (2004) used airborne hyperspectral image data to predict the electrical conductivity of soils. They found a correlation between 6_a and the hyperspectral reflectance signal of the vegetation with an $R^2 = 0.49$.

On the other hand, non-invasive geophysical methods such as frequency-domain electromagnetic-induction instruments (EMI) and gamma-ray spectrometry are rapid methods for assessing soil moisture patterns and physicochemical properties of the underlying substrate of plants (Corwin and Lesch, 2005; Tromp-van Meerveld and McDonnell, 2009; Robinson et al., 2012). EMI sensors measure the bulk electrical conductivity (ECa) of soils, which is affected by water content, mineralogy, texture, porosity, salinity, temperature, organic matter, and bulk density (Corwin and Lesch, 2005). Thus ECa measurements can provide spatially distributed information about soil properties. However, parameter relationships are non-unique and site-specific. Moreover, Werban et al. (2009) recommend the establishment of site-specific relationships between ECa and soil properties of the top soil with respect to seasonal effects. Robinson (2009) and Franz et al. (2011) successfully applied time lapse EMI measurements for isolating the water content signal from ECa.

With gamma-ray spectrometry, the natural gamma radiation of the topsoil is recorded. The texture as well as the mineralogy and the geological origin of source rocks are the main influencing factors affecting the nuclide concentration in sediments and soils. Consequently, gamma-ray measurements of single nuclides or their ratios were used in several studies to determine soil texture (Kiss et al., 1988; Martz and de Jong, 1990; Hyvönen et al., 2005). However, gamma-ray concentrations are influenced by other soil properties as well, for example, organic carbon content or pH (Dierke and Werban, 2013).

The application of multi-sensor approaches might be one way of overcoming ambiguous parameter relationships. Castrignano et al. (2012) tested the integration of EMI and gamma-ray spectrometry data, which proved to be very effective for interpreting soil variation by overcoming the weakness of every individual sensor. In any case, the establishment of parameter relationships between geophysical and soil parameters remains a critical issue.

However, geophysical parameter sets of soils provide soil-related information, for example, the recognition of patterns, even without transforming physical parameters into soil parameters. This information could be the key toward a better understanding of functional relationships on the landscape scale.

The main hypothesis for this work is that biochemical–biophysical plant characteristics in combination with geophysical observations can be used to identify soil heterogeneity and provide additional information for identifying functional heterogeneity. Plant-related variations in the study at hand investigate the feasibility of using the hyperspectral reflectance of the vegetation canopy to characterize, describe, and predict the physical–chemical components and the characteristics of the underlying soil. Therefore, different imaging hyperspectral index types, single band reflectance, and spectral indices are related to the geophysical soil parameters using regression models.

Data and Methods

Study Area

The area "Roßlauer Oberluch" used for the study approach is situated in Saxony-Anhalt, a region of Central Germany (Fig. 2 and 3). The area is part of the Terrestrial Environmental Observatories (TERENO) long-term monitoring region (Zacharias et al., 2011, 51.52° N lat, 12.16° E long).

The region "Roßlauer Oberluch" used to be an ancient floodplain and is made up of various flood channels, floodplain forests, and wet meadows (Scholz et al., 2009). From a geological perspective the study site can be assigned to the Holocene floodplain with the moraines of the Saale glacier to the North and bordered by the river Elbe to the South. Soils found in the "Roßlauer Oberluch" are predominantly very granulitic and silty (Krüger and Rupp, 2009). An overview of dominant soil texture classes, soil types, and biotope types is presented in Fig. 4a–4c. The groundwater level and soil water conditions in the "Roßlauer Oberluch" are determined by both precipitation and the flow regimes of the river Elbe and the river Rossel. The "Roßlauer Oberluch" is characterized by a high degree of variation in groundwater levels and soil water conditions, ranging from permanently flooded to areas with a groundwater level that is 275 cm below the surface (Krüger and Rupp, 2009).

Airborne Imaging Spectrometer Data

Imaging hyperspectral data sets of the test site "Roßlauer Oberluch" were performed using the hyperspectral sensors AISA-EAGLE/HAWK, (Fig. 5b, www.specim.fi) with a ground resolution of 2 m (recording date 23 September 2010) using a Cessna 207 (Fig. 5a). To record navigation data, we used the GPS/INS unit RT3102

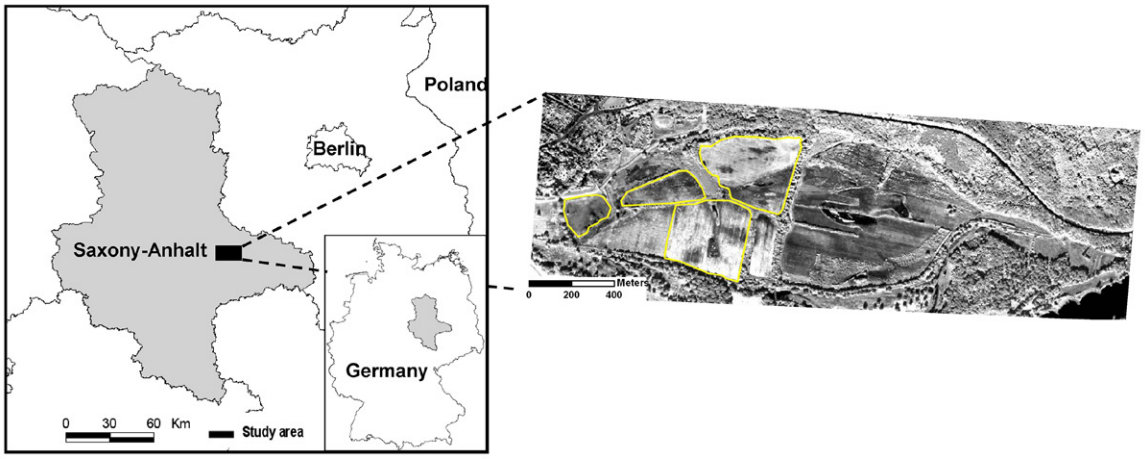

Fig. 2. Study area "Roßlauer Oberluch" situated in Saxony-Anhalt, Germany.

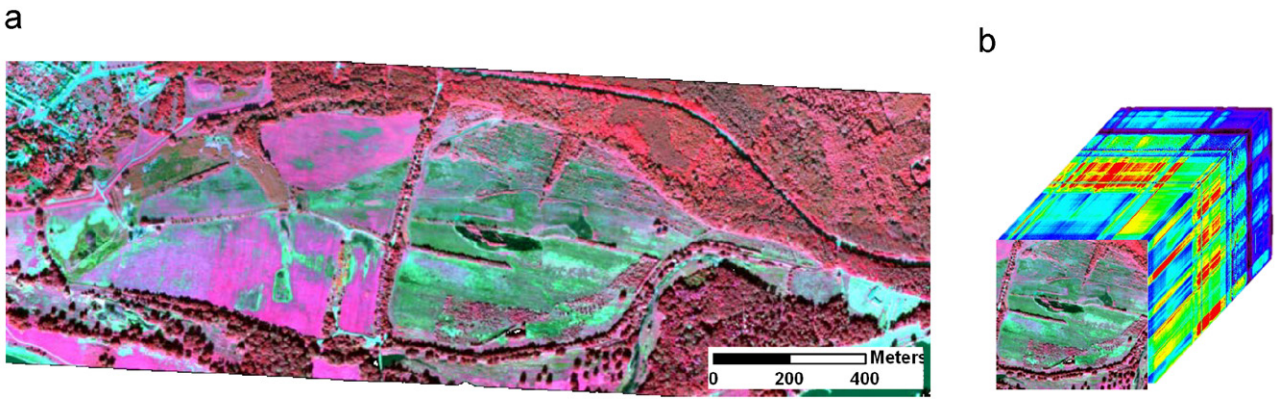

Fig. 3. (a) Color InfraRed (CIR)—image—region Rosslau—taken from the hyperspectral sensor AISA-EAGLE/HAWK, spectral range 400–2500 nm, 2 m ground resolution, 491 spectral bands, date of recording 23 Sep. 2010 with a Cessna 207, (b) Data cube—with 461 spectral bands.

(Oxford Technical Solutions Ltd, UK). Raw hyperspectral images were recorded and operated during the flight campaign using the specialized software RSCube (Spectral Imaging Ltd, Mäkisara, 1998). The specific parameters of the AISA-DUAL hyperspectral data recorded are shown in Table 1.

Data and Preprocessing

After the airborne AISA-EAGLE/HAWK (DUAL) raw data had been recorded, they were radiometric-corrected according to the CaliGeo procedure (Spectral Imaging Ltd, Mäkisara, 1998) run under ENVI (ITT Visual Information Solution, CO, USA). Following radiometric correction, an image-driven, radiometric recalibration and rescaling method was implemented to reduce ocular linear and nonlinear miscalibrations in the hyperspectral data, reduction of miscalibration effects (ROME) (Rogaß et al., 2011). Atmospheric correction was performed using the software ATCOR4 (Richter and Schläpfer, 2002) that had been modified to account for the specific band characteristics of the AISA sensors. A digital elevation model (DEM) was used together with the geocoding procedure CaliGeo for the orthorectification of the airborne hyperspectral image. After pre-processing, the hyperspectral data could then be referred to with a geo-code as ground reflectance data with a spatial ground resolution of 2 m.

Calculation of Spectral Vegetation Indices and Spectral Derivatives

Several indices and index types based on the imaging hyperspectral sensor AISA-DUAL were calculated and tested in terms of their suitability for predicting vegetation patterns as a function of soil and soil water conditions. The spectral vegetation indices (VI) used can be divided into two categories: (i) Reflectance vegetation indices—for these indices the reflectance value [$R_{(X)}$] at the central wavelength (x nm) of each band of the imaging AISA-EAGLE/HAWK spectrometer (400–2500 nm, 491 spectral bands) was used; and (ii) published vegetation indices—65 vegetation indices published in the relevant literature were tested. Spectral vegetation indices reflect the specific biochemical–physical characteristics of the vegetation and are categorized into different groups. In the current study those spectral indices in particular were applied that can act as indicators for mapping the "vitality" of plants.

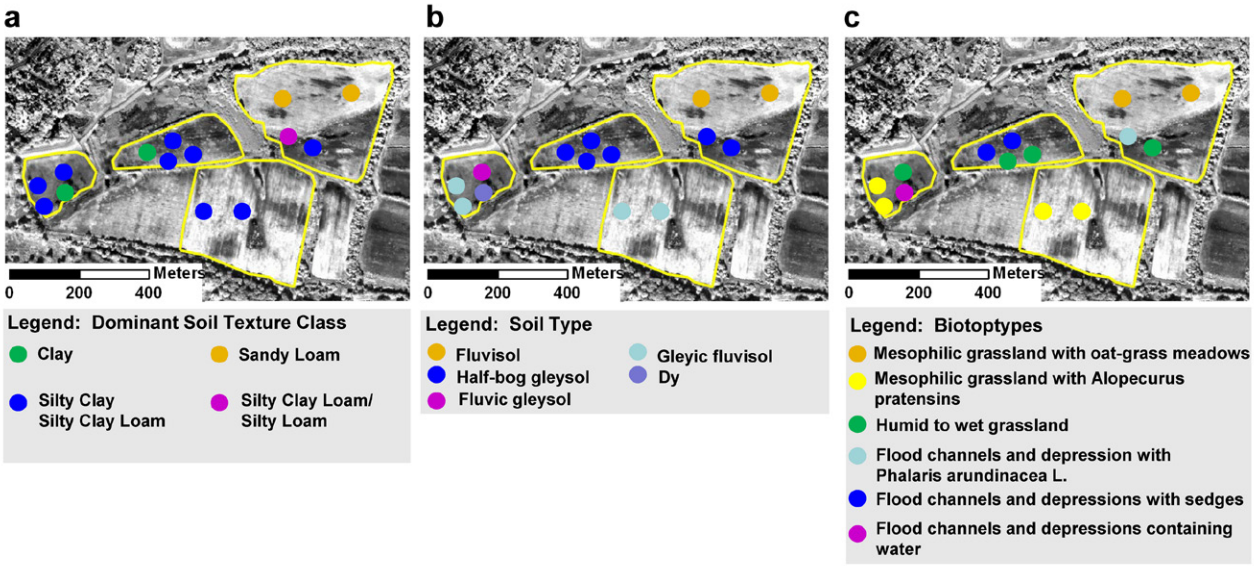

Fig. 4. Distribution of (a) dominant soil texture classes, (b) soil types, (c) biotoptypes in the study area "Roßlauer Oberluch" situated in Saxony-Anhalt, Germany (changed after Krüger and Rupp, 2009; Scholz et al., 2009).

We investigated the possibility of mapping (i) changes to the composition and the percentage of photosynthetically active pigments such as chlorophyll *a*, *b*, and xanthophylle; (ii) changes in measurements of photosynthesis activity through the fluorescence effects in plants; (iii) changes to the plant water status as well as the percentage of water in leaf cells; (iv) changes to cellulose and lignin content in the vegetation; and changes to plant transpiration, resulting in changes to leaf arrangement and geometry, stomata distribution as well as special protective mechanisms such as leaf hairs and cuticula structure.

Measurements of Soil Proxies

Mobile geophysical platforms were equipped with frequency-domain electromagnetic-induction instruments and a portable gamma-ray spectrometer. The devices were attached to sledges with a GPS and dragged along by a tractor (Fig. 6).

Electromagnetic Induction for Soil Mapping

The EMI method is a non-invasive technique to measure ECa. Measurements were performed in August 2009 after a period of 10 hot days with no rainfall using an EM38DD and an EM31 (both instruments from Geonics, Canada). These instruments transmit an alternating magnetic field (primary field) through a coil that induces a current (or secondary field) in the subsurface.

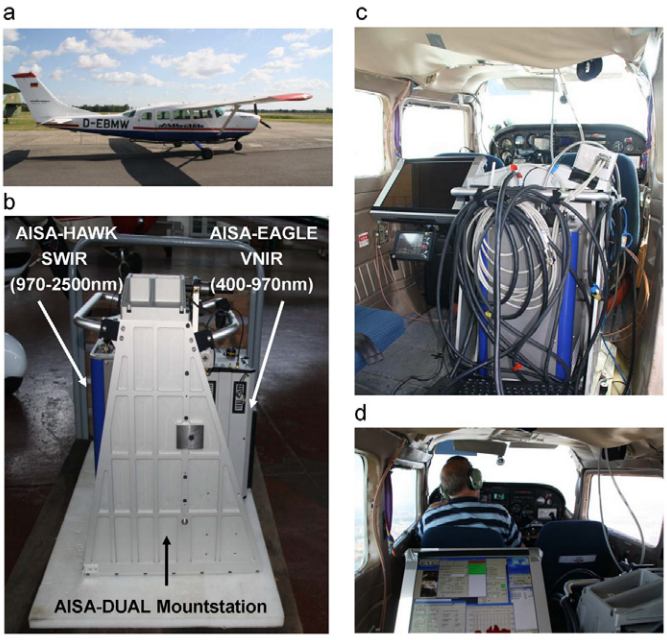

Fig. 5. (a) Recording hyperspectral data using a Cessna 207, (b) Hyperspectral sensors AISA-EAGLE/ASIA-HAWK (combined referred to as AISA-DUAL) are mounted onto a special mount station, (c) AISA-DUAL sensor in a Cessna 207, (d) Recording and operation of raw hyperspectral images using the specialized software RSCube (Spectral Imaging Ltd, Mäkisara, 1998).

Table 1. Specifications of the hyperspectral data AISA-EAGLE/HAWK (DUAL).

Recording date	Recording ground resolution	Focal length (EAGLE/ HAWK)	FOV	Swath	Spectral range	Spatial pixel	Spectral resolution	Spectral bands	Sensor	Platform
	m	cm	°	m	nm		nm			
23 Sept. 2010	2	18.5/22.5	36.7	300	400–2400	300	2.12–6.26	491	AISA-EAGLE/ HAWK (DUAL)	Aircraft-Cessna 206

A second coil receives both alternating magnetic fields and measures the quadrature phase (QP) from which the apparent electrical conductivity (ECa) can be calculated directly and the in-phase (Telford et al., 1990). During our investigation only QP measurements were taken. The instruments are widely used instruments for near-surface applications that measure both the vertical and horizontal dipole orientation, resulting in different effective depths of exploration (Callegary et al., 2007). The EM38DD consists of two separate EM38 instruments that are positioned perpendicularly to each other, enabling both horizontal and vertical dipole axes. The EM38DD has different sensitivities that depend on different soil depths. The vertical axis (EM38DD V) orientation is sensitive to deeper soil layers (maximum response from 0.3–0.6 m), while the horizontal axis (EM38DD H) orientation is mainly influenced by the near-surface soil layers (50% response from 0–0.5 m) (McNeill, 1980; Callegary et al., 2007). Measurements with a horizontal axis orientation are therefore more sensitive to the very near surface. Measurements with the EM31 were performed in vertical dipole orientation. EMI data were collected with a sampling rate of five records per second. The distance between the transects was approx. 12 m. After conducting a geostatistical variogram analysis, the data were interpolated using an ordinary kriging procedure.

The ECa measurements indicate the presence of fine structured patterns (Fig. 7a–7c) and a broad range of values from around 0 to above 100 mS m^{-1} (see Table 2). High ECa values (>40 mS m^{-1}) are related to flood plain channels and a flood plain depression in the far western area.

Gamma-ray Spectrometry for Soil Mapping

The concentration of gamma-ray emissions of soils depends on different soil properties, which are a function of the source rock and the processes during soil genesis under different climatic conditions as well as the effects of management (e.g., pH) and exogenous influences (e.g., soil moisture).

Fig. 6. Measurement arrangement of (a) gamma-ray spectrometer and (b) EM38DD.

Measured concentrations of the gamma-ray emitter Potassium ^{40}K and the decay series of Uranium ^{238}U and Thorium ^{232}Th can be used to differentiate between different types of hard rocks and to carry out sediment characterization. During radioactive decay, every nuclide emits gamma radiation depending on its specific typical discriminative energy. Radioactive decay is a statistical process. All radioactive decay occurs independently of other decay events and the time interval between decay events is not constant, which leads to a statistical noise within the measured data. Gamma-ray spectrometers count the decay rate (intensity) of the specific energy being released during each decay. To calculate the concentration

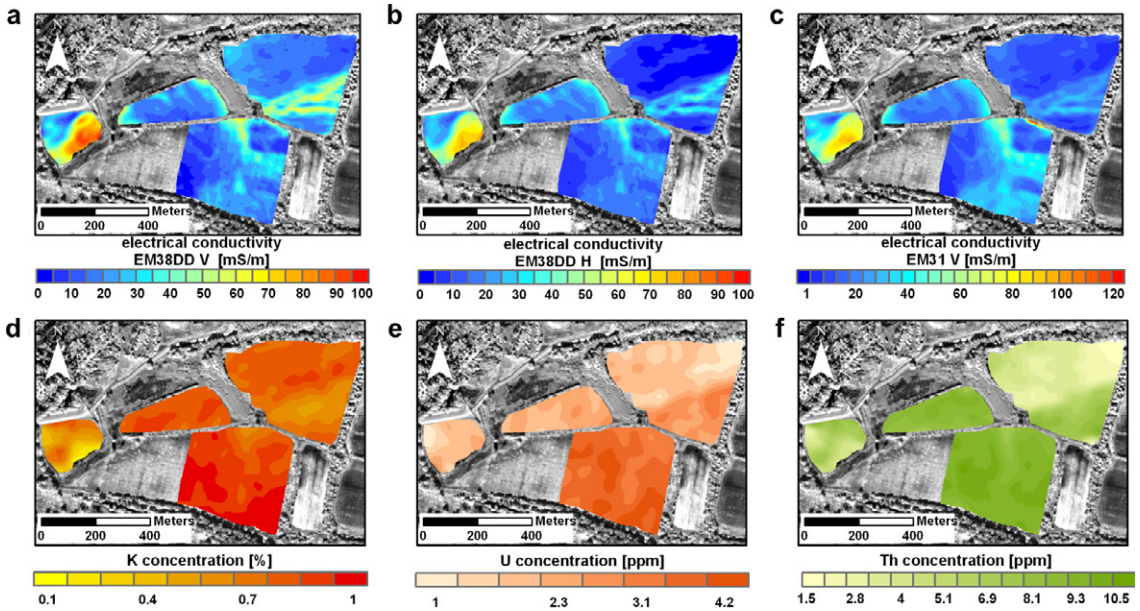

Fig. 7. Interpolated data of (a) EM38DD V, vertical dipole, (b) EM38DD H, horizontal dipole, (c) EM31 V, vertical dipole, (d) gamma-ray spectrometer, K concentration, (e) gamma-ray spectrometer, U concentration, and (f) gamma-ray spectrometer, Thorium concentration.

Table 2. Descriptive statistics geophysical data: EMI, gamma-ray spectrometry.

Variable	Penetration depth	Min	Max	Mean	Median	SD
	m					
EM38DD H, mS m^{-1}	Integral up to 0.70 (Callegary et al., 2007)	0	82.9	17.7	15.7	13.7
EM38DD V, mS m^{-1}	Integral up to 1.5 (Callegary et al., 2007)	2.4	99.5	25.1	20.2	15.8
EM31 V, mS m^{-1}	Integral up to 4–6 (Callegary et al., 2007)	1.5	125.2	20.8	16.2	16.0
γK, %	Integral up to 0.3 (Cook et al., 1996)	0.0	1.1	0.7	0.8	0.1
γU, ppm	Integral up to 0.3 (Cook et al., 1996)	1	4.2	2.7	2.5	0.8
γTh, ppm	Integral up to 0.3 (Cook et al., 1996)	1.5	10.2	6.8	7.9	2.5

of Th and U, the progeny of their decay series is taken. To perform inverse calculations from progeny concentrations back to Th and U concentrations, it is assumed that the measured decay series is in equilibrium (IAEA, 2003). The measured concentration is influenced by soil moisture. An increase in soil moisture will decrease the measured gamma-ray concentration due to attenuation of the radiation by water. In a soil with a bulk density of 1.6 g/cm^3 most of the measured gamma rays (90%) originate from the top 30 cm of soil and 50% from the top 10 cm (Cook et al., 1996).

The field measurements were performed using a portable gamma-ray spectrometer with a 4-L thallium-activated NaI (Sodium iodide) crystal from GF Instruments with an automatic peak stabilization. The detector records the energy spectrum between 100 keV and 3 MeV divided into 512 channels. It was calibrated to calculate the concentration of ^{40}K [%], ^{238}U [ppm], and ^{232}Th [ppm]. The detector was mounted onto a sledge at a height of 30 cm with GPS positioning so that it could be towed by four-wheel drive vehicles across the field sites. A counting period of 5 s was applied. This resulted in a point distance of approx. 7 m within the driven transects. The distance between the transects was approx. 12 m.

A spatial filtering process was applied to the data to reduce statistical noise, to improve statistical certainty of the variogram analysis and of the ordinary kriging interpolation.

Gamma-ray concentrations of the study site show less detailed structures than the ECa values. Nevertheless the mapped areas show distinct patterns of varying nuclide concentrations (see Fig. 7). The very northeastern area stands out with a high concentration of K and a low concentration of Th resulting in a differing Th/K relationship compared to all other mapped areas. From a pedogenetical perspective, the northeastern part is characterized by glacio-fluviatile deposits, while all other areas are covered by recent alluvial deposits.

Statistical Model Approach

The predictive power of spectral and spatial vegetation patterns with regard to underlying soil and soil water conditions (as described by the geophysically measured proxies EMI and gamma-ray spectrometry) was assessed by means of a statistical analysis. Univariate and multivariate linear regression models were used to develop the respective transfer functions. We used a resampling framework to account for the large sample size (n = 82,150, grain size 2 × 2 m). We randomly resampled 1000 responses and their respective predictor variables 1000 times from the original data for each hyperspectral band, spectral indicators, and spectral derivatives separately. These were used in a robust regression framework to down-weigh the influence of potential outliers. For each of these 1000 models per predictor, the calculated coefficients and their respective standard errors, t values, and error probabilities were recorded. Finally mean values were calculated.

The goodness of fit of the models with the primary variables (ECa, γK, γTh, γU) were analyzed using the R^2 and the RMSE of the model averages.

The calculation for all spectral indices, spectral published indices and index derivatives of imaged hyperspectral data were performed using IDL/ENVI, v.4.8. The statistical analyses were performed using R 2.15.2 with the packages MASS (function rlm) and qpcR (function RMSE).

Results

Relationship between Geophysically Measured Soil Proxies and Plant Reflectance Spectra

To investigate the ability to predict spatial patterns of geophysical proxies from plant reflectance, the correlation between the spectral and the geophysical data was calculated. The resulting correlograms are provided in Fig. 8a–8d.

The highest correlation between electrical conductivity and the spectral information can be found in the wavelength range from 695–700 nm with an R^2 of approximately 0.3 (RMSE = 11.33 mS m^{-1}) for EM 38DD H (Fig. 8a and 8b). EM38DD H is characterized by the shallowest penetration depth and the highest sensitivity to the very near surface soil properties compared to EM38DD V and EM31. Clearly lower linear correlations exist for

the electrical conductivity measured by EM38DD V and EM31 V (R^2 of max. 0.26).

For the analysis of every single spectral wavelength in terms of nuclide concentration of K in the "Roßlauer Oberluch" the best model fit obtained an R^2 of 0.35 and an RMSE of 0.12% with a spectral wavelength of 750 nm (Fig. 8b and 8c). Th and U are much less correlated to the measured spectra.

Relationship between the Geophysically Measured Soil Proxies and Spectral Vegetation Indices

To analyze the relationship between geophysically measured soil characteristics against hyperspectral reflectance information, we tested 65 well known published spectral vegetation indices. In the current study those spectral indices were selected that are indicators for quantifying and imaging the "vitality" of plants. Changes to the biochemical–physical characteristics of plants in this respect refer to changes in the plants' photosynthetic pigments, photosynthesis activity, water status and water content, lignin, and cellulose content and the transpiration of plants and vegetation.

For the electrical conductivity, the Plant Senescence Reflectance Index (PSRI) (Merzlyak et al., 1999) was found to have the highest correlation of all tested indices. For EM38DD H and EM38DD V a R^2 of 0.39 was achieved (Table 3). PSRI was also the most predictive index for EM31DD V, but the correlation was significantly lower than for the EMI measurements (R^2 = 0.28). The relationship between PSRI and the EMI measurements also becomes clearly visible by comparing their spatial distributions (Fig. 9). The Cellulose Absorption Index (CAI) (Daughtry et al., 1996) also provided a reasonable fit for EM38DD H with an R^2 of 0.39. Furthermore, the CAI predicts EM38DD V with an R^2 of 0.40 (RMSE 12.17 m Sm^{-1}).

To assess soil properties measured by gamma-ray spectrometry, the best model fit was displayed by the Triangular Vegetation Index (TVI) (Broge and Leblanc, 2001) for γK with an R^2 of 0.37 and an RMSE of 0.18%. For γTh and γU none of the tested indices was able to provide a reasonable prediction.

The Normalized Difference Vegetation Index (NDVI) is one of the oldest and most frequently used vegetation indices for quantifying the greenness of vegetation. Our results demonstrate that the

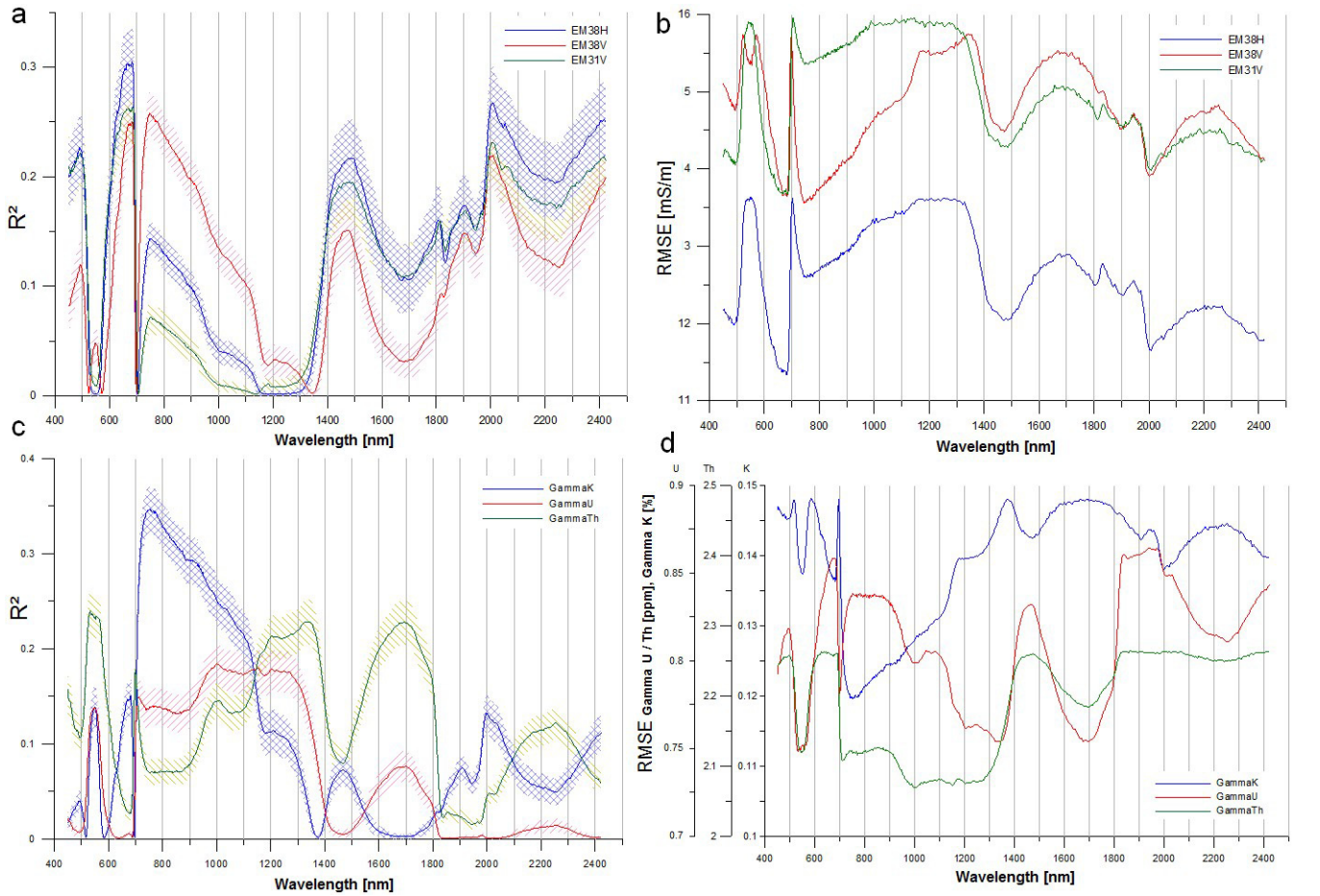

Fig. 8. (a) Best model fits for each spectral wavelength with EM38DD H, horizontal dipole, EM38DD V, vertical dipole and EM31 V, vertical dipole, (b) RMSE for EMI measurements, (c) best model fits for each spectral wavelength with gamma-ray spectrometry, K concentration, gamma-ray spectrometry, U concentration, and gamma-ray spectrometry, Thorium concentration, (d) RMSE for gamma-ray spectrometry measurements.

Table 3. Best model fits for univariate regression between EMI and gamma-ray spectrometry measurements and spectral vegetation indices derived from the imaging hyperspectral sensor AISA-EAGLE/HAWK in "Roßlauer Oberluch."

	EM38DD H R^2 RMSE	EM38DD V R^2 RMSE	EM31 V R^2 RMSE	γTh R^2 RMSE	γK R^2 RMSE	γU R^2 RMSE
	mS m^{-1}			ppt	%	ppt
Published spectral indices						
PSRI—Plant senescence Reflectance index $[(R_{680} - R_{500})/R_{750}]$ Group: Pigment activity/Light use efficiency Merzlyak et al. (1999), Sims and Gamon (2003)	0.39 [10.65]	0.39 [12.22]	0.28 [13.46]	0.09 [2.41]	0.27 [0.13]	0.006 [0.80]
CAI—Cellulose absorption Index $[0.5\ (R_{2000}+R_{2200})-R_{2100}]$ Group: Leaf content Daughtry et al. (1996)	0.39 [10.63]	0.40 [12.17]	0.27 [13.64]	0.101 [2.42]	0.33 [0.12]	0.02 [0.79]
TVI—Triangular vegetation Index $0.5[120(R_{750} - R_{550}) - 200(R_{670} - R_{550})]$ Group: Pigment activity/light use efficiency: Broge and Leblanc (2001)	0.22 [12.04]	0.32 [12.93]	0.13 [14.87]	0.04 [2.37]	0.37 [0.18]	0.12 [0.75]
NPCI $(R_{680}-R_{430})/(R_{680}+R_{430})$ Group: Pigment activity/light use efficiency: Penuelas et al. (1994)	0.02 [13.53]	0.12 [14.78]	0.003 [15.90]	0.25 [2.09]	0.248 [0.13]	0.25 [0.69]
Frequently used indices						
NDVI $(R_{800}-R_{670})/(R_{800}+R_{670})$ Group: Greenness Rouse et al. (1974)	0.34 [11.03]	0.38 [12.42]	0.23 [13.95]	0.001 [2.43]	0.29 [0.125]	0.02 [0.79]

NDVI has a mean predictive power for EM 38DD V with an R^2 of 0.38 and for EM38DD H with an R^2 of 0.34.

Figure 10 displays the wavelengths of the most predictive spectral bands. The majority of these spectral wavelengths can be assigned to leaf pigments. EMI results measured using EM38DD also shows some dependencies with plant water content, while γU and γK are additionally related to wavelengths that represent plant cell structure properties.

Relationship between the Geophysically Measured Soil Characteristics and Terrain Characteristics

Modeling of Proxies for Soil Properties

Geomorphological characteristics such as profile curvatures are known to have a strong influence on soil distribution and properties and have been used in numerous studies to explain the variability of soil variables (e.g., Florinsky et al., 2002; Gessler et al., 2000; Grunwald, 2009; McBratney et al., 2003; Schmidt et

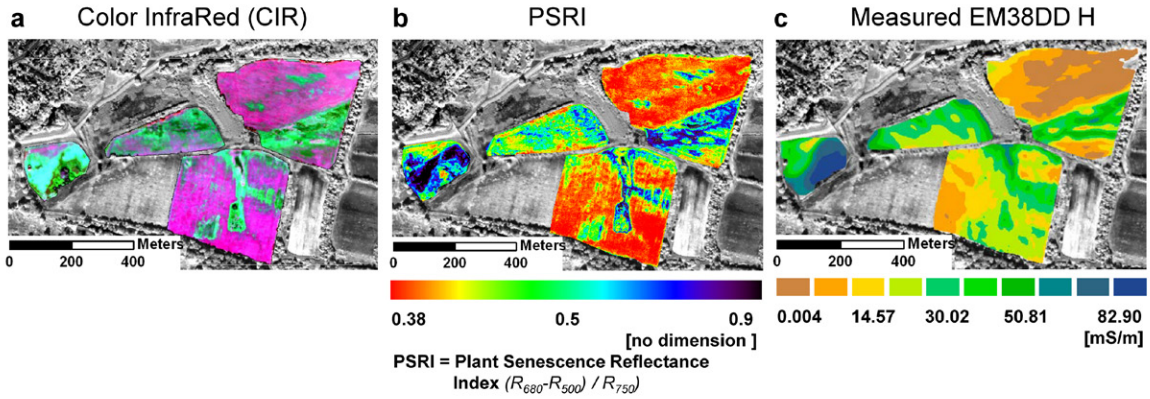

Fig. 9. Test site "Roßlauer Oberluch", (a) Color Infrared image (CIR)—taken from the hyperspectral sensor AISA-EAGLE/HAWK, 400–2500 nm, 2 m ground resolution, 461 spectral bands, date of recording 23 Sep. 2010 with a Cessna 207, (b) Plant Senescence Reflectance Index (PRSI) derived from AISA-EAGLE/HAWK spectral information, best model fit for EM38DD H against PSRI with R^2 = 0.39 (RMSE = 10.65 mS/M^{-1}), (c) Measured and interpolated electrical conductivity—EM38DD H.

al., 2010; Scull et al., 2003). To develop a predictive model for geophysical properties using hyperspectral measurements, it has been tested to which extent the prediction can be improved by including elevation information as an additional variable. Therefore, two statistical classification analysis procedures were conducted using the commercial statistics software SPSS (SPSS Inc., 2010). The first step was to calculate the coefficient of determination values between the geographical elevation, the different geophysical properties, and the selected spectral wavelengths and spectral indices. From the respective correlation matrix (Table 4) it can be postulated that significant negative correlations exist between the mean geographical elevation and the measured electrical conductivity and that elevation seems to be more predictive than the hyperspectral information. A weaker, but still significant (0.001 probability level) correlation exists between the elevation and the gamma-ray spectrometry values. Furthermore, the correlation matrix also indicates a stronger correlation between geographical elevation and the spectral indices PSRI, CAI, and the wavelengths 520 and 680 nm.

To reduce information redundancies and take into account intercorrelation between the variables, a stepwise multiple regression procedure was performed. In this procedure, multiple regression is performed a number of times, whereby each time the weakest correlated variable is removed. At the same time the variance inflation factor (VIF) according to the stepwise introduction of predictor variables was calculated, which enables the detection of multicollinearities (or collinearities) between the predictor variables. VIF provides a measure of the degree to which a regression coefficient is affected by information redundancies between the predictor variables. Variables with VIF values greater than 5 were removed from the model. The results from the stepwise multiple regression analysis are displayed in Table 3 and Fig. 11.

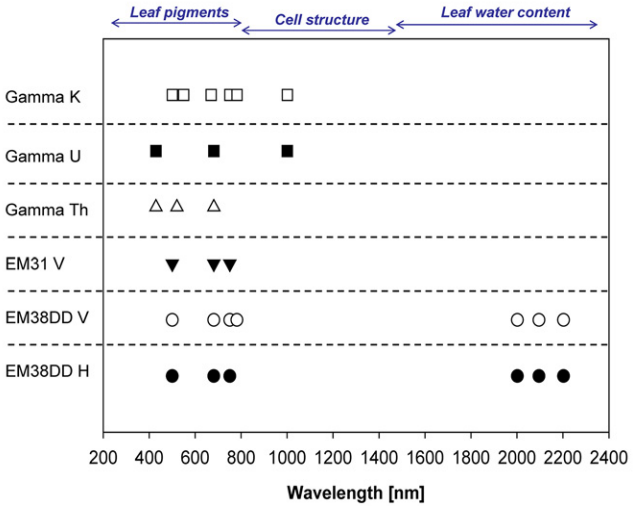

Fig. 10. Positions of the best spectral predictors (spectral indices, spectral derivatives, spectral wavelengths) showing their individual wavelengths between 450 and 2480 nm for the best model fits when predicting EM38DD H, EM38DD V, EM31 V, γTh, γU, and γK.

The results (Table 5) show that integrating spectral indices or spectral wavelengths into elevation-based models leads to only small improvements in the predictive power for the EMI values. As already indicated by the correlation matrix, most of the explained variance for predicting EMI values is based on elevation. The regression approach that was applied indicates that in combination with elevation information, NPCI is the most effective spectral index for the prediction of EMI values. This is interesting because the correlation between NPCI and the EMI-measurements is much weaker than for other tested spectral indices (see Table 4). However, unlike the other spectral indices, there is hardly any correlation between NPCI and the geographical elevation and the

Table 4. Matrix of correlation between the best model variables from hyperspectral data, EM and gamma-ray and morphology in the "Roßlauer Oberluch."

	Elevation	520 nm	680 nm	780 nm	1000 nm	PSRI	CAI	NPCI	TVI	EM38DD H	EM38DD V	EM31 V	γTh	γU	γK
Elevation	1														
520 nm		1													
680 nm		0693	1												
780 nm		0255	−0456	1											
1000 nm		0489	−0184	0923	1										
PSRI	0656	−0303	−0803	0682	0474	1									
CAI	−0628	0131	0686	−0789	−0644	−0873	1								
NPCI	0002	−0353	0225	−0616	−0619	−0334	0402	1							
TVI	0420	0052	−0623	0921	0800	0832	−0862	−0623	1						
EM38DD H	−0798	0268	0553	−0371	−0202	−0623	0624	0132	−0465	1					
EM38DD V	−0647	0072	0505	−0500	−0367	−0631	0638	0348	−0573	0915	1				
EM31 V	−0696	0313	0513	−0261	−0097	−0534	0519	0048	−0362	0919	0852	1			
γTh	−0530	0461	0164	0265	0386	−0095	0022	−0514	0209	0205	−0073	0179	1		
γU	−0341	0252	−0066	0372	0430	0075	−0135	−0501	0344	0060	−0100	0112	0833	1	
γK	0371	0103	−0387	0586	0506	0526	−0576	−0507	0610	−0558	−0713	−0445	0475	0502	1

integration of NPCI into the elevation-based model results in the largest increase in predictive information. This observation also became evident from the results of a principal components analysis, which was conducted before each regression analysis. In any case the first two principal components (PC) explained about 80% of the total variance and elevation and NPCI are among the leading components of PC 1 and 2, respectively. NPCI introduces a maximum of "new" information regarding the variability of the dataset. This finding also demonstrates the benefit of combining covariance analysis and principal component analysis. Collinearities, information redundancies, and predicitive quality are sometimes difficult to detect from using covariance analysis alone.

For EM31 V, elevation alone explains about 50% of the total variation and no significant improvement could be found by integrating further spectral information.

For the gamma-ray measurements the findings were slightly different. Whereas for these data as well the elevation shows a significant predictive power, its contribution to explaining the overall variability of the geophysical proxies is much lower than for the EMI measurements. This was already indicated by the correlation coefficient matrix where the gamma-ray measurements showed a lower correlation with the geographical elevation than the EMI measurements. In contrast to the EMI prediction equations, for γK and γU the spectral index TVI improved the predictive model. In the case of γK, TVI was the most predictive variable and explained about 40% of the total variability.

In Fig. 11a–11h the measurements and predictions of EM38DD H, EM38DD V, and γK using the best predictive models are displayed graphically. Figures 11a, 11c, 11e, and 11g show the spatial distribution of the measured geophysical parameters. Figures 11b, 11d, 11f, and 11h integrate the best spectral wavelengths, the best spectral indicators as well as elevation in the multivariate models.

Discussion

The general aim of the presented study was to investigate whether the spectral and spatial patterns of plants and vegetation can be used as proxies for soil properties measured by electromagnetic induction and gamma-ray spectrometry.

The best correlations found (EM38DD H—spectral range 680 nm/2000 nm, R^2 = 0.3; γK—wavelength 780 nm, R^2 = 0.35) correspond with findings of Zipprich et al. (2001) and Li et al. (2011) based on a handheld non-imaging hyperspectral sensor. The comparison of electrical conductivity measured with EM38DD V and EM31 V against the spectral reflectance of the vegetation resulted in a correlation of around R^2 = 0.25. This weaker correlation can be explained by the larger penetration depth of the last two EM techniques (penetration depth of EM38DD H is up to 0.7 m with a high sensitivity to the very top, while EM38DD V is up to 1.5 m and EM31 V is between 4 and 6 m). This indicates the stronger relationship between plant properties and properties of the upper soil horizons. By testing different spectral indices the best model fits could be achieved with the Plant Senescence Reflectance Index (PSRI) (Merzlyak et al., 1999) for EM38DD H (R^2 0.39) and EM38DD V (R^2 0.39). The PSRI (R680-R500)/R750 is designed to maximize the sensitivity of the index to the ratio of bulk carotenoids (α and β-carotene) to chlorophyll. According to Merzlyak et al. (1999) an increase in PSRI reflects an increment of canopy stress. For this reason the PSRI is often used to monitor the vitality of vegetation and to detect plant physiological stress (Liew et al., 2008; Stagakis et al., 2010; Clark et al., 2011). To predict EM38DD H (R^2 0.39) and EM 38DD V (R^2 0.40) a good model fit was also achieved using the CAI. The CAI $[0.5(R_{2000}+R_{2200})-R_{2100}]$ describes the average depth of the cellulose absorption feature at 2.1 μm in the reflectance spectra (Daughtry et al.,1996). Nagler et al. (2000, 2003) were able to demonstrate different amounts of cellulose in the vegetation as a function of soil water content by using the vegetation index CAI.

The best model fit for predicting the gamma-ray concentration as a soil proxy was quantified for γK using the TVI. This relationship might be indirectly caused by a high influence of plant available K at this study site. Such a relationship between γK and plant available K was already shown by Wong and Harper (1999) and Pracilio et al. (2006). The TVI after Broge and Leblanc (2001) calculates the relative difference between red and near-infrared reflectance in conjunction with the magnitude of reflectance in the green region, developed by the fact that the total area of the triangle (green, red, infrared) will increase as a result of chlorophyll absorption. The spectral index TVI is an important indicator for characterizing the biochemical chlorophyll content of vegetation (Haboudane et al., 2004).

Among the tested spectral indices also the most frequently used vegetation index, the NDVI was tested in terms of its predictive power of EMI or gamma-ray spectrometry measurements. When compared to other spectral indicators, the NDVI also proved to be a good predictor for electromagnetic induction EM38DD V with an R^2 of 0.38 and an RMSE = 12.42.

The complete analysis of the specific positions of all spectral predictors for EMI and gamma-ray nuclides showed spectral indicators and index derivatives in the range of 420 to 800 nm to be highly sensitive to predict soil characteristics. Spectral information from the short wave infrared (SWIR) from 2000 to 2200 nm was only sensitive for predicting EM38DD H and EM38DD V. This shows that in particular the spectral ranges of the maximal chlorophyll absorption (440–500 nm, 650–700 nm) as well as the red edge (680–700 nm) contain relevant information to be directly related to soil properties. This can be explained as vegetation stress indication which is spectrally detectable due to changes in biochemical–biophysical vegetation properties. According to Naumann et al. (2008) and Zarco-Tejada et al. (2009) vegetation stress leads to

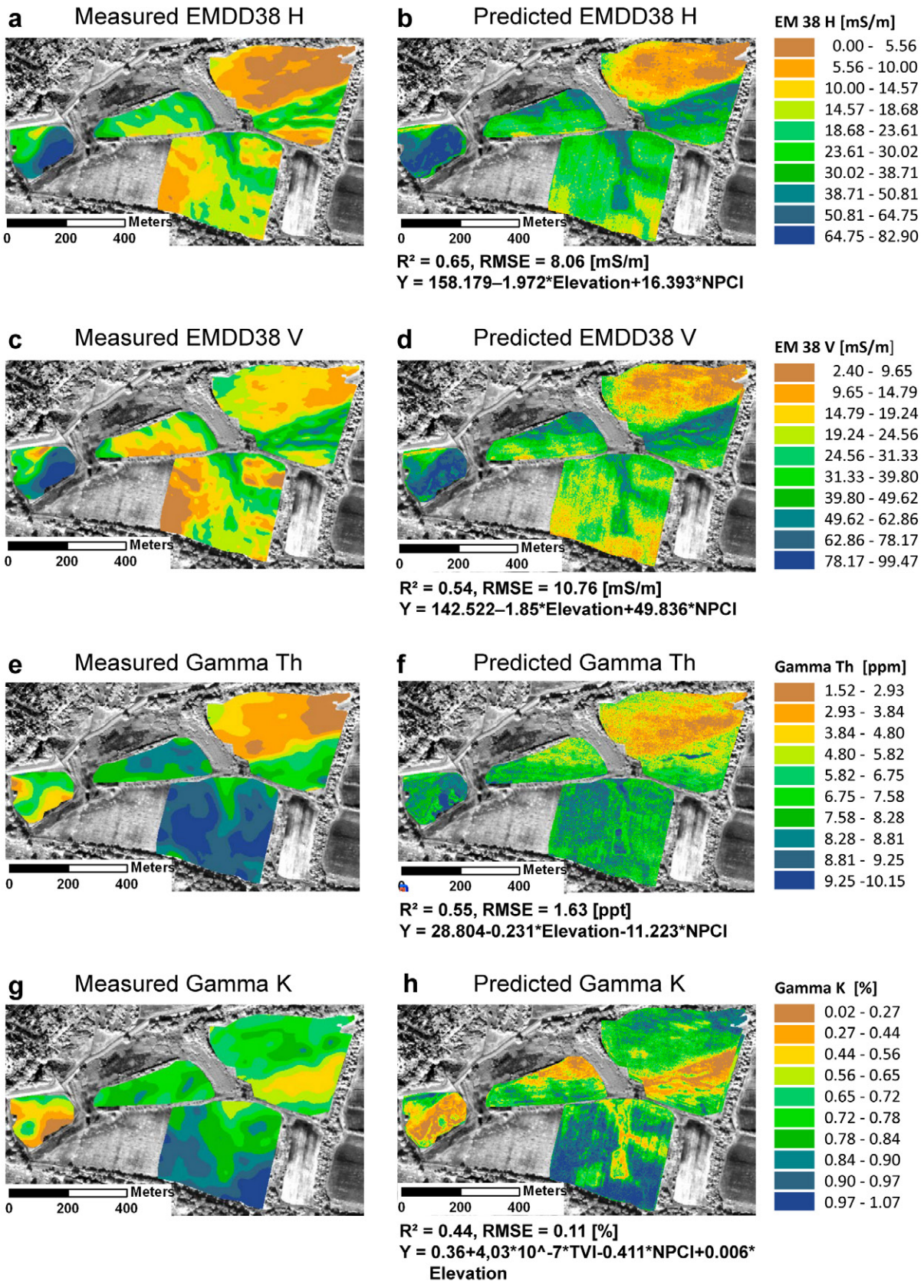

Fig. 11. The best model fits for mulitvariate regression between EM38DD H, EM38DD V, γTh and γK and information from hyperspectral bands of the imaging AISA-EAGLE/HAWK sensor, (a) measured—EM38DD H, (b) Predicted—EMDD38 H, (c) measured—EMDD38 V, (d) Predicted—EM38DD V, (e) measured—γTh, (f) Predicted—γTh, (g) measured—γK, (h) Predicted—γK.

changes in the composition and proportion of photosynthetically active pigments such as chlorophyll *a*, *b*, and xanthophylle as well as changes in photosynthetic activity. Use of the spectral range between 2000 and 2200 nm for predicting EM38DD H and EM38DD V also delivers information about the change in the water status of plants. In the past many authors have confirmed the sensitivity of the short wave infrared spectral region II (SWIR) in the spectral range from 2000 to 2500 nm for measuring leaf water content, cellulose, and lignin content of plants (Sims and Gamon, 2003; Bannari et al., 2007; Cheng et al., 2008). Similarly, investigations on the vegetation water content of corn and soybeans conducted by Cheng et al. (2008) using MODIS remote sensing data resulted in an R^2 of 0.74 in the spectral range of 1640 nm and an R^2 of 0.72 in the range of 2130 nm. Both Champagne et al. (2003) and Cheng et al. (2008) used hyperspectral data for estimating plant water content with SWIR spectral information.

Table 5. Best models for univariate and multivariate regression between EM and gamma-ray spectrometry measurements and variables in the "Roßlauer Oberluch."

Predicted variable	Best model fits	R^2	RMSE
EM38DD H	$Y = 164{,}994 - 1971 \times$ Elevation	0.637	8.26
	$Y = 158{,}179 - 1972 \times$ Elevation $+ 16{,}393 \times$ NPCI	0.655	8.06
EM38DD V	$Y = 163{,}241 - 1848$ x Elevation	0.419	12.10
	$Y = 142{,}522 - 1850 \times$ Elevation $+ 49{,}836 \times$ NPCI	0.540	10.76
EM31 V	$Y = 171{,}351 - 2014 \times$ Elevation	0.485	11.54
γTh	$Y = 24{,}138 - 0232 \times$ Elevation	0.281	2.06
	Y	0.545	1.64
γK	$Y = 0584 + 7729 \times 10^{-7}$ TVI	0.373	1.64
	$Y = 0733 + 6100 \times 10^{-7} \times$ TVI $- 2{,}75 \times$ NPCI	0.399	0.11
	$Y = 0360 + 4034 \times 10^{-7} \times$ TVI $- 0411 \times$ NPCI $+ 0{,}006 \times$ Elevation	0.439	0.11
γU	$Y = 4211 - 3635 \times$ NPCI	0.251	0.70
	$Y = 7898 - 3631 \times$ NPCI $- 0{,}490 \times$ Elevation	0.363	0.64
	$Y = 8396 - 1815 \times$ NPCI $- 0074 \times$ Elevation $+ 2766 \times 10^{-6}$ TVI	0.437	0.60

The most important factor for the predictive models (Table 5) to explain the variance of all EMI and γray measurement signals is the elevation information. Our measurements suggest that the floodplain is characterized by different stages of soil moisture even after a hot, dry period. Soil moisture is very closely related to the geomorphology and substrate in the investigation area, see Fig. 11a–11h. This is reflected by the EMI and gamma-ray measurements. The EM31 V could only be predicted with the variable elevation with an R^2 of 0.49 (RMSE = 11.54). The hyperspectral information does not contribute to predicting EM31 V (Table 5). The best prediction was obtained for EM38DD H with an R^2 of 0.65 (RMSE = 8.06) as well as for EM38DD V with an R^2 of 0.54 (RMSE = 10.76). Elevation and the spectral indicator NPCI improve the model fit. The application of time-lapse EMI could be a possibility to overcome the influence of soil moisture on the ECa measurements in the next step of investigations.

Parameters measured by gamma-ray spectrometry are mainly dominated by substrate types and less by soil water content. A good predictive model for γTh ($R^2 = 0.55$, RMSE = 1.64) results from integrating spectral parameters NPCI and elevation. This effect is based on the high dependency of Th on the substrates with different pedogenesis at the field site, for example, low γTh concentration in the northeastern area dominated by sandy glacio-fluviatil sediments and higher γTh concentration in clay-rich alluvial deposits. According to investigations conducted by different authors (Kiss et al., 1988; Martz and de Jong, 1990; van der Klooster et al., 2011) γTh shows very good correlations between the soil type "clay" and gamma-ray activity. For γK and γU the inclusion of elevation and hyperspectral indices TVI and NPCI improve the model fit. To predict γK an R^2 of 0.44 (RMSE = 0.11) was obtained and for γU an R^2 of 0.44 (RMSE = 0.60) was obtained. Gamma K is less influenced by the type of substrate than by the plant available K in the Roßlau area. Gamma U is generally more affected by soil moisture (Dierke and Werban, 2013), however flood channels seem to have no influence on γU at this particular field site.

Hence, areas with depressions with increased clay content display a higher water storage capacity than the more sandy areas, which again is reflected in a change in the spectral reflectance of the vegetation.

Conclusions and Outlook

Soil conditions like bulk density or organic matter content and soil water conditions influence the biochemical–physical properties in vegetation as a result of adaptation or plant stress or the distribution of vegetation structures (Lausch et al., 2012). The results show that hyperspectral remote sensing is a suitable tool to describe and analyze biochemical vegetation characteristics in relation to underlying soil properties. As expected, electrical conductivity of soils is determined to a large degree by relief properties and therefore relief information should be included in the modeling process. It can be assumed that the coherences between biochemical vegetation, soil properties, and soil water conditions are nonlinear. For this reason, we intend to test further classification approaches such as SVM, PLSR, and cluster algorithms in the next step. This will also include additional spatial information of descriptive soil-related site characteristics such as soil water budget information.

Acknowledgments

The research was supported by TERENO. This work was supported by iSOIL, Interactions between soil related sciences—linking geophysics, soil science, and digital soil mapping, which is a collaborative project (grant agreement number 211386) co-funded by the Research DG of the European Commission within the RTD activities of the FP7 Thematic Priority Environment; iSOIL is one member of the SOIL TECHNOLOGY CLUSTER of research projects funded by the EC. We would like to thank our technicians for assistance with the field measurements.

References

Bajwa, S., P. Bajcsy, P. Groves, and L. Tian. 2004. Hyperspectral image data mining for band selection in agricultural applications. Trans. ASAE 47:895–907.

Bannari, A., K.S. Khurshid, K. Staenz, and J.W. Schwarz. 2007. A comparison of hyperspectral chlorophyll indices for wheat crop chlorophyll content estimation using laboratory reflectance measurements. IEEE Trans. Geosci. Rem. Sens. 45:3063–3074. doi:10.1109/TGRS.2007.897429

Bannari, A., A. Pacheco, K. Staenz, H. McNairn, and K. Omari. 2006. Estimating and mapping crop residues cover on agricultural lands using hyperspectral and IKONOS data. Remote Sens. Environ. 104:447–459. doi:10.1016/j.rse.2006.05.018

Ben-Dor, E., K. Patkin, A. Banin, and A. Karnieli. 2002. Mapping of several soil properties using DAIS-7915 hyperspectral scanner data: A case study over clayey soils in Israel. Int. J. Remote Sens. 23:1043–1062. doi:10.1080/01431160010006962

Bouma, J. 2009. Soils are back on the global agenda: Now what? Geoderma 150:224–225. doi:10.1016/j.geoderma.2009.01.015

Bouma, J., J. Stoorvogel, B.J. van Alphen, and H.W.G. Booltink. 1999. Pedology, precision agriculture, and the changing paradigm of agricultural research. Soil Sci. Soc. Am. J. 63:1763–1768. doi:10.2136/sssaj1999.6361763x

Broge, N.H., and E. Leblanc. 2001. Comparing prediction power and stability of broadband and hyper-spectral vegetation indices for estimation of green leaf area index and canopy chlorophyll density. Remote Sens. Environ. 76:156–172. doi:10.1016/S0034-4257(00)00197-8

Callegary, J.B., T.P.A. Ferre, and R.W. Groom. 2007. Vertical spatial sensitivity and exploration depth of low-induction-number electromagnetic-induction instruments. Vadose Zone J. 6:158–167. doi:10.2136/vzj2006.0120

Castrignano, A., M.T.F. Wong, M. Stelluti, D. De Benedetto, and D. Sollitto. 2012. Use of EMI, gamma-ray emission and GPS height as multi-sensor data for soil characterisation. Geoderma 175–176:78–89. doi:10.1016/j.geoderma.2012.01.013

Champagne, C.M., K. Staenz, A. Bannari, H. Mcnairn, and J.-C. Deguise. 2003. Validation of a hyperspectral curve-fitting model for the estimation of plant water content of agricultural canopies. Remote Sens. Environ. 87:148–160. doi:10.1016/S0034-4257(03)00137-8

Chang, D.-H., and S. Islam. 2000. Estimation of soil physical properties using remote sensing and artificial neural network. Remote Sens. Environ. 74:534–544. doi:10.1016/S0034-4257(00)00144-9

Cheng, Y.-B., S.L. Ustin, D. Riaño, and V.C. Vanderbilt. 2008. Water content estimation from hyperspectral images and MODIS indexes in Southeastern Arizona. Remote Sens. Environ. 112:363–374. doi:10.1016/j.rse.2007.01.023

Clark, M.L., D. Roberts, J.J. Ewel, and D.B. Clark. 2011. Estimation of tropical rain forest aboveground biomass with small-footprint lidar and hyperspectral sensors. Remote Sens. Environ. 115:2931–2942. doi:10.1016/j.rse.2010.08.029

Claudio, H.C., Y. Cheng, D.A. Fuentes, J.A. Gamon, H. Luo, W. Oechel, H.-L. Qiu, A.F. Rahman, and D.A. Sims. 2006. Monitoring drought effects on vegetation water content and fluxes in chaparral with the 970 nm water band index. Remote Sens. Environ. 103:304–311. doi:10.1016/j.rse.2005.07.015

Cook, S.E., R.J. Corner, P.R. Groves, and G.J. Grealish. 1996. Use of airborne gamma radiometric data for soil mapping. Aust. J. Soil Res. 34:183–194. doi:10.1071/SR9960183

Corwin, D., and S. Lesch. 2005. Apparent soil electrical conductivity measurements in agriculture. Comput. Electron. Agric. 46:11–43. doi:10.1016/j.compag.2004.10.005

Daughtry, C.S.T., J.E. McMurtrey, III, E.W. Chappelle, W.J. Hunter, and J.L. Steiner. 1996. Measuring crop residue cover using remote sensing techniques. Theor. Appl. Climatol. 54:17–26. doi:10.1007/BF00863555

Dierke, C., and U. Werban. 2013. Relationships between gamma-ray data and soil properties at an agricultural test site. Geoderma 199:90–98. doi:10.1016/j.geoderma.2012.10.017

Eitel, J.U.H., P.E. Gessler, A.M.S. Smith, and R. Robberecht. 2006. Suitability of existing and novel spectral indices to remotely detect water stress in *Populus* spp. For. Ecol. Manage. 229:170–182. doi:10.1016/j.foreco.2006.03.027

Ellenberg, H., H.E. Weber, R. Düll, V. Wirth, W. Werner, and D. Paulißen. 1991. Zeigerwerte von Pflanzen in Mitteleuropa. Scr. Geobotanica 18:1–248.

Feilhauer, H., and S. Schmidtlein. 2011. On variable relations between vegetation patterns and canopy reflectance. Ecol. Inform. 6:83–92. doi:10.1016/j.ecoinf.2010.12.004

Florinsky, I.V., R.G. Eilers, G.R. Manning, and L.G. Fuller. 2002. Prediction of soil properties by digital terrain modelling. Environ. Model. Softw. 17:295–311. doi:10.1016/S1364-8152(01)00067-6

Franz, T.E., E.G. King, K.K. Caylor, and D.A. Robinson. 2011. Coupling vegetation organization patterns to soil resource heterogeneity in a central Kenyan dryland using geophysical imagery. Water Resour. Res. 47:W07531. doi:10.1029/2010WR010127

Gessler, P.E., O.A. Chadwick, F. Chamran, L. Althouse, and K. Holmes. 2000. Modeling soil-landscape and ecosystem properties using terrain attributes. Soil Sci. Soc. Am. J. 64:2046–2056. doi:10.2136/sssaj2000.6462046x

Grayson, R., and G. Blöschl. 2001. Spatial patterns in catchment hydrology: Observations and modelling. Cambridge Univ. Press, Cambridge, UK.

Grunwald, S. 2009. Multi-criteria characterization of recent digital soil mapping and modeling approaches. Geoderma 152:195–207. doi:10.1016/j.geoderma.2009.06.003

Haboudane, D., J.R. Miller, E. Pattey, P.J. Zarco-Tejada, and I.B. Strachan. 2004. Hyperspectral vegetation indices and novel algorithms for predicting green LAI of crop canopies: Modeling and validation in the context of precision agriculture. Remote Sens. Environ. 90:337–352. doi:10.1016/j.rse.2003.12.013

Hák, R., H.K. Lichtenthaler, and U. Rinderle. 1990. Decrease of the chlorophyll fluorescence ratio F 690/F 730 during greening and development of leaves. Radiat. Environ. Biophys. 29:329–336. doi:10.1007/BF01210413

Haubrock, S.-N., S. Chabrillat, M. Kuhnert, P. Hostert, and H. Kaufmann. 2008. Surface soil moisture quantification and validation based on hyperspectral data and field measurements. Appl. Remote Sens. 2. doi:10.1117/1.3059191

Hernández-Clemente, R., R.M. Navarro-Cerrillo, L. Suárez, F. Morales, and P.J. Zarco-Tejada. 2011. Assessing structural effects on PRI for stress detection in conifer forests. Remote Sens. Environ. 115:2360–2375. doi:10.1016/j.rse.2011.04.036

Heuvelink, G.B.M., and R. Webster. 2001. Modelling soil variation: Past, present, and future. Geoderma 100:269–301. doi:10.1016/S0016-7061(01)00025-8

Hill, M.O., D.B. Roy, J.O. Mountford, and R.G.H. Bunce. 2000. Extending Ellenberg's indicator values to a new area: An algorithmic approach. J. Appl. Ecol. 37:3–15. doi:10.1046/j.1365-2664.2000.00466.x

Hyvönen, E.T.P., E. Vanhanen, H. Arkumaa, and R. Sutinen. 2005. Airborne gamma-ray surveys in Finland. Geological Survey of Finland. In: M.-L. Airo, editor, Aerogeophysics in Finland 1972–2004: Methods, system characteristics and application. Geol. Surv. Finland Spec. Pap. 39:119–134.

IAEA. 2003. Guidelines for radioelement mapping using gamma ray spectrometry data. IAEA-TECDOC-1363. IAEA, Vienna, Austria.

Jackson, R.D., R.J. Reginato, and S.B. Idso. 1976. Timing of ground truth acquisition during remote assessment of soil-water content. Remote Sens. Environ. 4:249–255.

Jarmer, T., Lavée, H., Sarah, P. and Hill, J. 2005. The use of remote sensing for the assessment of soil inorganic carbon in the Judean Desert (Israel). In: A. Röder and J. Hill, editors, Proceedings of the 1st International Conference on Remote Sensing and Geoinformation Processing in the Assessment of Land Degradation and Desertification (RGLDD). Univ. of Trier, Trier, Germany. pp. 68–75.

King, E.G., T.E. Franz, and K.K. Caylor. 2012. Ecohydrological interactions in a degraded two-phase mosaic dryland: Implications for regime shifts, resilience, and restoration. Ecohydrology 5(6):733–745. doi:10.1002/eco.260

Kiss, J.J., E. de Jong, and J.R. Bettany. 1988. The distribution of natural radionuclides in native soils of southern Saskatchewan, Canada. J. Environ. Qual. 17:437–445. doi:10.2134/jeq1988.00472425001700030016x

Kowalsky, M.B.S., Y. Finsterle, and Y. Rubin. 2004. Estimating flow parameter distributions using ground-penetrating radar and hydrological measurements during transient flow in the vadose zone. Adv. Water Resour. 27:583–599. doi:10.1016/j.advwatres.2004.03.003

Krüger, F., and H. Rupp. 2009. Bodenkundliche Sondierung ausgewählter Standorte im Roßlauer Oberluch und bei Klieken. Landesamt für Umweltschutz (Hrsg) Naturschutz im Land Sachsen– Anhalt, 46 Jahrgang, Sonderheft. pp. 116–124.

Lausch, A., M. Pause, I. Merbach, S. Gwillym-Margianto, K. Schulz, S. Zacharias, and R. Seppelt. 2012. Scale-specific hyperspectral remote sensing approach in environmental research. Photogram. Fernerkund. Geoinf. 5:589–602.

Lausch, A., M. Pause, I. Merbach, S. Zacharias, D. Doktor, M. Volk, and R. Seppelt. 2013a. A new multi-scale approach for monitoring vegetation using remote sensing-based indicators in laboratory, field and landscape. Environ. Monit. Assess. 185:1215–1235. doi:10.1007/s10661-012-2627-8

Lausch, A., M. Pause, A. Schmidt, C. Salbach, S. Gwillym Margianto, and I. Merbach. 2013b. High temporal monitoring of biochemical and biophysical vegetation parameters over an entire growing period of spring barley using an imaging spectrometer in the laboratory. Can. J. Rem. Sens. 39(3) 1–17.

Li, D., Q. Guo, J.P.J.A. Rahilly, G.M. Phelps, and T.C. Harmon. 2011. Correlation between soil apparent electroconductivity and plant hyperspectral reflectance in a managed wetland. Int. J. Remote Sens. 32:2563–2579. doi:10.1080/01431161003698427

Liew, O.W., R.C.J. Chong, B. Li, and A.K. Asundi. 2008. Signature optical cues: Emerging technologies for monitoring plant health. Sensors (Basel Switzerland) 8:3205–3239. doi:10.3390/s8053205

Lin, H.S., W. Kogelmann, C. Walker, and M.A. Bruns. 2006. Soil moisture patterns in a forested catchment: A hydropedological perspective. Geoderma 131:345–368. doi:10.1016/j.geoderma.2005.03.013

Lin, H., D. Wheeler, J. Bell, and L. Wilding. 2005. Assessment of soil spatial variability at multiple scales. Ecol. Modell. 182:271–290. doi:10.1016/j.ecolmodel.2004.04.006

Mäkisara, K. 1998. AISA data user's guide. Research Note 1894. Tech. Res. Centre of Finland, Espoo, Finland. pp. 1–54.

Martz, L.W., and E. de Jong. 1990. Natural radionuclides in the soils of a small agricultural basin in the Canadian prairies and their association with topography, soil properties and erosion. Catena 17:85–96. doi:10.1016/0341-8162(90)90017-8

McBratney, A.B., M.L.M. Santos, and B. Minasny. 2003. On digital soil mapping. Geoderma 117:3–52. doi:10.1016/S0016–7061(03)00223–4

McNeill, J.D. 1980. Electromagnetic terrain conductivity measurement at low induction numbers. Technical Note TN-6. Geonics Ltd., Ontario, Canada. p. 15.

Merzlyak, M.N., A.A. Gitelson, O.B. Chivkunova, and V.Y. Rakitin. 1999. Nondestructive optical detection of pigment changes during leaf senescence and fruit ripening. Physiol. Plant. 106:135–141. doi:10.1034/j.1399-3054.1999.106119.x

Miller, J.R., G.H. Mohammed, T.L. Noland, and P.H. Sampson. 2002. Vegetation stress detection through chlorophyll a + b estimation and fluorescence effects on hyperspectral imagery. J. Environ. Qual. 31:1433–1441. doi:10.2134/jeq2002.1433

Nagler, P.L., C.S.T. Daughtry, and S.N. Goward. 2000. Plant litter and soil reflectance. Remote Sens. Environ. 71:207–215. doi:10.1016/S0034-4257(99)00082-6

Nagler, P.L., E.P. Glenna, A.L. Russ, and C.S.T. Daughtry. 2003. Cellulose absorption index (CAI) to quantity mixed soil-plant litter scenes. Remote Sens. Environ. 87:310–325. doi:10.1016/j.rse.2003.06.001

Naumann, J.C., J.E. Anderson, and D.R. Young. 2008. Linking physiological responses, chlorophyll fluorescence and hyperspectral imagery to detect salinity stress using the physiological reflectance index in the coastal shrub, Myrica cerifera. Remote Sens. Environ. 112:3865–3875. doi:10.1016/j.rse.2008.06.004

Pause, M., K. Schulz, S. Zacharias, and A. Lausch. 2012. Near-surface soil moisture estimation by combining airborne L-band brightness temperature observations and imaging hyperspectral data at the field scale. J. Appl. Remote Sens. 6:063516. doi:10.1117/1.JRS.6.063516

Penuelas, J., Gamon, J.A., Fredeen, A.L., Merino, J., and Field, C.B. 1994. Reflectance indexes associated with physiological-changes in nitrogenlimited and water-limited sunflower leaves. Remote Sensing Environ. 48: 135–146. doi:10.1016/0034-4257(94)90136-8.

Pracilio, G., M.L. Adams, K.R.J. Smettem, and R.J. Harper. 2006. Determination of spatial distribution patterns of clay and plant available potassium contents in surface soils at the farm scale using high resolution gamma ray spectrometry. Plant Soil 282:67–82. doi:10.1007/s11104-005-5229-1

Richter, R., and D. Schläpfer. 2002. Geo-atmospheric processing of airborne imaging spectrometry data. Part 2: Atmospheric/topographic correction. Int. J. Remote Sens. 23:2631–2649. doi:10.1080/01431160110115834

Robinson, D.A., H. Abdu, I. Lebron, and S.B. Jones. 2012. Imaging of hill-slope soil moisture wetting patterns in a semi-arid oak savanna catchment using time-lapse electromagnetic induction. J. Hydrol. 416:39–49.

Robinson, D.A., I. Lebron, B. Kocar, K. Phan, M. Sampson, N. Crook, and S. Fendorf. 2009. Time-lapse geophysical imaging of soil moisture dynamics in tropical deltaic soils: An aid to interpreting hydrological and geochemical processes. Water Resour. Res. 45(1): W00D32. doi:10.1029/2008WR006984.

Rogaß, C., D. Spengler, M. Bochow, K. Segl, A. Lausch, D. Doktor, S. Roessner, R. Behling, H.-U. Wetzel, and H. Kaufmann. 2011. Reduction of radiometric miscalibration—Applications to pushbroom sensors. Sensors (Basel Switzerland) 11:6370–6395. doi:10.3390/s110606370

Rouse, J.W., Jr., Hass, R.H., Schell, J.A., and Deering, D.W. 1974. Monitoring vegetation systems in the Great Plains with ERTS. In: Proceedings Earth Resources Technology Satellite (ERTS) Symposium, 3rd, Greenbelt, MD, 10–14 Dec. 1973. NASA SP-351, NASA, Washington, D.C. pp. 309–317.

Schmidt, K., T. Behrens, K. Friedrich, and T. Scholten. 2010. A method to generate soilscapes from soil maps. J. Plant Nutr. Soil Sci. 173:163–172. doi:10.1002/jpln.200800208

Schmidtlein, S. 2005. Imaging spectroscopy as a tool for mapping Ellenberg indicator values. J. Appl. Ecol. 42:966–974. doi:10.1111/j.1365-2664.2005.01064.x

Schmidtlein, S., H. Feilhauer, and H. Bruelheide. 2012. Mapping plant strategy types using remote sensing. J. Veg. Sci. 23:395–405. doi:10.1111/j.1654-1103.2011.01370.x

Schmidtlein, S., and J. Sassin. 2004. Mapping of continuous floristic gradients in grasslands using hyperspectral imagery. Remote Sens. Environ. 92:126–138. doi:10.1016/j.rse.2004.05.004

Schulz, K., R. Seppelt, E. Zehe, H.J. Vogel, and S. Attinger. 2006. Importance of spatial structures in advancing hydrological sciences. Water Resour. Res. 42: W03S03. doi:10.1029/2005WR004301

Scholz, M., H. Rupp, G. Puhlmann, Ch. Ilg, M. Gerisch, F. Dziock, K. Follner, F. Foeckler, J. Glaeser, F. Konjuchow, F. Kruger, A. Regner, E. Schwarze, W.V. Tumpling, S. Duquesne, M. Liess, U. Werban, S. Zacharias, and K. Henle. 2009. Deichrückverlegungen in Sachsen-Anhalt und wissenschaftliche Begleituntersuchungen am Beispiel des Roslauer Oberluchs. Landesamt für Umweltschutz (Hrsg): Naturschutz im Land Sachsen– Anhalt, 46 Jahrgang, Sonderheft. pp. 103–116.

Scull, P., J. Franklin, O.A. Chadwick, and D. McArthur. 2003. Predictive soil mapping: A review. Prog. Phys. Geogr. 27:171–197. doi:10.1191/0309133303pp366ra

Shrestha, R. 2006. Relating soil electrical conductivity to remote sensing and other soil properties for assessing soil salinity in northeast Thailand. Land Degrad. Dev. 17:677–689. doi:10.1002/ldr.752

Sims, D.A., and J.A. Gamon. 2003. Estimation of vegetation water content and photosynthetic tissue area from spectral reflectance: A comparison of indices based on liquid water and chlorophyll absorption features. Remote Sens. Environ. 84:526–537. doi:10.1016/S0034-4257(02)00151-7

Stagakis, S., N. Markos, O. Sykioti, and A. Kyparissis. 2010. Monitoring canopy biophysical and biochemical parameters in ecosystem scale using satellite hyperspectral imagery: An application on a Phlomis fruticosa Mediterranean ecosystem using multiangular CHRIS/PROBA observations. Remote Sens. Environ. 114:977–994. doi:10.1016/j.rse.2009.12.006

Suárez, L., P.J. Zarco-Tejada, G. Sepulcre-Cantó, O. Pérez-Priego, J.R. Miller, J.C. Jiménez-Muñoz, and J. Sobrino. 2008. Assessing canopy PRI for water stress detection with diurnal airborne imagery. Remote Sens. Environ. 112:560–575. doi:10.1016/j.rse.2007.05.009

Swatantran, A., R. Dubayah, D. Roberts, M. Hofton, and J.B. Blair. 2011. Mapping biomass and stress in the Sierra Nevada using lidar and hyperspectral data fusion. Remote Sens. Environ. 115:2917–2930. doi:10.1016/j.rse.2010.08.027

Telford, W.M., L.P. Geldart, and R.E. Sheriff. 1990. Applied geophysics. Cambridge Univ. Press, Cambridge, UK.

Tromp-van Meerveld, H.J.T., and J.J. McDonnell. 2009. Assessment of multi-frequency electromagnetic induction for determining soil moisture patterns at the hillslope scale. J. Hydrol. 368:56–67. doi:10.1016/j.jhydrol.2009.01.037

van der Klooster, E., F.M. van Egmond, and M.P.W. Sonneveld. 2011. Mapping soil clay contents in Dutch marine districts using gamma-ray spectrometry. Eur. J. Soil Sci. 62:743–753. doi:10.1111/j.1365-2389.2011.01381.x

van Egmond, F.M., P. Dietrich, U. Werban, and U. Sauer. 2009. iSOIL: Exploring the soil as the basis for quality crop production and food security. Qual. Assur. Saf. Crop. Foods 1:117–120. doi:10.1111/j.1757-837X.2009.00019.x

Vereecken, H., J.A. Huisman, H. Bogena, J. Vanderborght, J.A. Vrugt, and J.W. Hopmans. 2008. On the value of soil moisture measurements in vadose zone hydrology: A review. Water Resour. Res. 44. doi:10.1029/2008WR006829.

Wehrhan, M., M. Sommer, M. Zipprich, U. Weller, W. zu Castell, and S. Ehrich. 2001. Erfassung mesoskaliger Bodenheterogeniten mit Hilfe flugzeuggestützter Fernerkundung. Mitt. Dtsch. Bodenkundl. Gesell. 96:569–570.

Werban, U., K. Kuka, and I. Merbach. 2009. Correlation of electrical resistivity, electrical conductivity and soil parameters at a long-term fertilization experiment. Near Surf. Geophys. 7:5–14.

Wigneron, J.P., J.C. Calvet, T. Pellarin, A.A. Van de Griend, M. Berger, and P. Ferrazzoli. 2003. Retrieving near-surface soil moisture from microwave radiometric observations: Current status and future plans. Remote Sens. Environ. 85:489–506. doi:10.1016/S0034-4257(03)00051-8

Wong, M.T.F., and R.J. Harper. 1999. Use of on-ground gamma-ray spectrometry to measure plant-available potassium and other topsoil attributes. Aust. J. Soil Res. 37:267–277. doi:10.1071/S98038

Zacharias, S., H. Bogena, L. Samaniego, M. Mauder, R. Fuß, T. Pütz, M. Frenzel, M. Schwank, C. Baessler, K. Butterbach-Bahl, O. Bens, E. Borg, A. Brauer, P. Dietrich, I. Hajnsek, G. Helle, R. Kiese, H. Kunstmann, S. Klotz, J. C. Munch, H. Papen, E. Priesack, H. P. Schmid, R. Steinbrecher, U. Rosenbaum, G. Teutsch, and H. Vereecken. 2011. A network of terrestrial environmental observatories in Germany. Vadose Zone J. 10:955–973. doi:10.2136/vzj2010.0139

Zarco-Tejada, P.J., J.A.J. Berni, L. Suárez, G. Sepulcre-cantó, F. Morales, and J.R. Miller. 2009. Remote sensing of environment imaging chlorophyll fluorescence with an airborne narrow-band multispectral camera for vegetation stress detection. Remote Sens. Environ. 113:1262–1275. doi:10.1016/j.rse.2009.02.016

Zarco-Tejada, P.J., V. González-Dugo, and J. Berni. 2012. Fluorescence, temperature and narrow-band indices acquired from a UAV platform for water stress detection using a micro-hyperspectral imager and a thermal camera. Remote Sens. Environ. 117:322–337. doi:10.1016/j.rse.2011.10.007

Zhang, Y., J.M. Chen, J.R. Miller, and T.L. Noland. 2008. Leaf chlorophyll content retrieval from airborne hyperspectral remote sensing imagery. Remote Sens. Environ. 112:3234–3247. doi:10.1016/j.rse.2008.04.005

Zipprich, M., W. zu Castell, M. Sommer, U. Weller, M. Wehrhan, and S. Ehrich. 2001. EM38- Ein Tool zur Erkennung von Bodenmustern. Mitt. Dtsch. Bodenkundl. Gesell. 96:581–582.